Supplementary Information for

Residual resistivity as an independent indicator of resonant levels in semiconductors

Bartlomiej Wiendlocha[1,*], Shantanu Misra[2], Anne Dauscher[2], Bertrand Lenoir[2], Christophe Candolfi[2,+]

[1] Faculty of Physics and Applied Computer Science, AGH University of Science and Technology, Aleja Mickiewicza 30, 30-059 Krakow, Poland
[*]E-mail: wiendlocha@fis.agh.edu.pl

[2]Institut Jean Lamour, UMR 7198 CNRS – Université de Lorraine, 2 allée André Guinier-Campus ARTEM, BP 50840, 54011 Nancy Cedex, France
[+]E-mail: christophe.candolfi@mines-nancy.univ-lorraine.fr

Content

1). Two-valence-band model

The valence band structure of SnTe can be modelled by considering that mainly two bands contribute to the transport: a parabolic heavy-hole band and a non-parabolic light-hole band, referred to as hereafter using the subscripts *hh* and *lh*, respectively. Assuming acoustic phonon scattering as the main scattering mechanism at 300 K, the thermopower is expressed as

$$S_{lh+hh} = \frac{k_B}{e}\frac{\xi\left({}^{1}_{.}F^{1}_{-2}(\eta,\alpha) - \eta\,{}^{0}_{.}F^{1}_{-2}(\eta,\alpha)\right) + \left({}^{1}_{.}F^{1}_{-2}(\eta-\Delta_V,0) - (\eta-\Delta_V)\,{}^{0}_{.}F^{1}_{-2}(\eta-\Delta_V,0)\right)}{\xi\,{}^{0}_{.}F^{1}_{-2}(\eta,\alpha) + {}^{0}_{.}F^{1}_{-2}(\eta-\Delta_V,0)}$$

where $\Delta_V = \Delta E/k_B T$ is the energy offset between the two valence band maxima. In this relation, the choice $\alpha = 0$ makes the heavy-hole band parabolic. $\alpha = k_B T/E_g$ is the non-parabolicity parameter, E_g is the energy gap and T is the temperature. In this relation, the functions ${}^{n}_{.}F^{m}_{l}$ are the generalized Fermi integral given by:

$${}^{n}_{.}F^{m}_{l} = \int_0^\infty \left(-\frac{\partial f}{\partial \varepsilon}\right)\varepsilon^n(\varepsilon+\alpha\varepsilon^2)^m[(1+2\alpha\varepsilon)^2+2]^{l/2}d\varepsilon$$

where f is the Fermi-Dirac distribution and ε is the reduced energy of the carriers. The parameter ξ is defined as

$$\xi = \frac{m^*_{hh}D^2_{hh}}{m^*_{lh}D^2_{lh}}$$

where m^*_{hh} is the density-of-states effective mass of the heavy valence band, m^*_{lh} is the density-of-states effective mass of the light valence band, D_{hh} is the heavy-valence-band acoustic deformation potential and D_{hh} is the light-valence-band acoustic deformation potential. The equations for hole concentrations are:

$$p_{hh} = \frac{1}{3\pi^2}\left(\frac{2{m_{hh}}^* k_B T}{\hbar^2}\right)^{3/2} {}^{0}_{.}F^{3/2}_{0}(\eta-\Delta_V,0)$$

$$p_{lh} = \frac{1}{3\pi^2}\left(\frac{2{m_{lh}}^* k_B T}{\hbar^2}\right)^{3/2} {}^{0}_{.}F^{3/2}_{0}(\eta,\alpha)$$

The Hall factors A_{lh} and A_{hh} of the light and heavy-hole band, respectively, are given by:

$$A_{hh} = \frac{3}{2} F_{1/2} \frac{F_{-1/2}}{2{F_0}^2}$$

$$A_{lh} = \frac{3K(K+2)}{(2K+1)^2} \frac{{}^0F_{-4}^{1/2}\,{}^0F_0^{3/2}}{({}^0F_{-2}^{1})^2}$$

where F_i are the Fermi integrals of order i and $K = m_{\parallel}^*/m_{\perp}^*$ is the ratio between the effective mass due to the anisotropy of the valence band at the L point of the Brillouin zone. These two effective masses are related to the density-of-states effective mass via:

$$m^* = N_V^{2/3}\left({m_{\perp}^*}^2 m_{\parallel}^*\right)^{1/3}$$

where N_V is the band degeneracy. The total Hall hole concentration p_H is then given by:

$$p_H = \frac{[bp_{lh} + p_{hh}]^2}{[A_{lh}b^2 p_{lh} + A_{hh}p_{hh}]}$$

where b is the mobility ratio between the light-hole and heavy-hole valence bands.

In the calculations of the Ioffe-Pisarenko curve, we used the following values for the various band parameters, determined by fitting experimental values in Ref. 21 of the main text: $E_g = 0.18$ eV, $m_{lh} = 0.14m_0$, $m_{hh} = 1.7m_0$, $\Delta_V = 0.40$ eV, $K = 4$, $b = 4$, $N_{V,lh} = 4$ and $N_{V,hh} = 12$. The values of Δ_V, m_{lh} and m_{hh} slightly differ from those originally used by Brebrick *et al.* (0.35 eV, $0.168m_0$ and $1.92m_0$, respectively). However, the above-mentioned values enable to better account for the experimental data obtained on several series of doped and self-doped (that is, by Sn vacancies) SnTe samples. This model nevertheless yields qualitatively similar Ioffe-Pisarenko curves with its characteristic hump at high hole concentrations evidencing the important contribution of the second valence band to the transport.

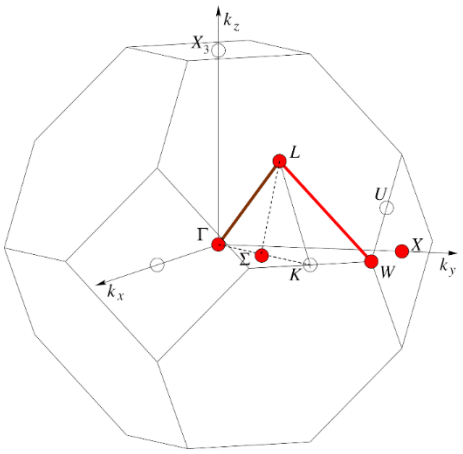

Figure S1. Brillouin zone of the rock-salt, face -centered -cubic structure of SnTe, with the high-symmetry points labelled. The "Σ point" corresponds to the point, which is in the middle between the Γ and K points, a frequently -used convention in the literature [see *e.g.* S1, S2].

2). Experimental and computational details

All the polycrystalline samples measured herein are those used in our previous study [S3]. Polycrystalline samples of $Sn_{1.03-x}In_xTe$ with nominal compositions x = 0.0, 0.0005, 0.0015, 0.0025, 0.0035, 0.0045, 0.0075, 0.0100 and 0.0200 were synthesized from direct reaction of stoichiometric quantities of elemental Sn, In and Te (5N, 99.999%) in evacuated silica tubes. Excess Sn was used to partly counterbalance the Sn vacancy concentration inherent to SnTe. The tubes, sealed under high vacuum, were placed in a vertical rocking furnace for 10h at 1100 K. before being quenched in room-temperature water. The obtained ingots were hand-ground into fine powders inside an argon-filled glove box and subsequently consolidated by Spark Plasma Sintering (SPS) in a graphite die at 750 K for 10 mins under an uniaxial pressure of 65 MPa. All the samples show a relative density of more than 96% of the theoretical density. The dense cylindrical pellets were then cut into rectangular bar-shaped samples of typical dimensions 8×2×2 mm^3 for transport property measurements.

Electrical resistivity and Hall effect were measured at 5 K using the ac transport option of a physical property measurement system (PPMS, Quantum Design). The Hall resistivity ρ_H was determined by measurements of the transverse electrical resistivity ρ_{xy} under magnetic field reversal following the relation $\rho_H = \left[\rho_{xy}(+\mu_0 H) - \rho_{xy}(-\mu_0 H)\right]/2$. The Hall coefficient R_H was derived from the slope of the $\rho_H(\mu_0 H)$ data for fields $-1 \leq \mu_0 H \leq 1$T. The Hall carrier concentration p_H and the Hall mobility μ_H were determined from the single-band relations $p_H = r_H/R_H e$ and $\mu_H = R_H/\rho$ where e is the electron charge and r_H is the Hall factor. In non-degenerate samples, this factor can significantly deviate from the conventionally-used value of 1, depending on the main scattering mechanism (r_H can vary up to 1.18 and 1.93 for acoustic phonon and ionized impurity scattering, respectively). In contrast, in degenerate samples, the deviations are less significant and the values of r_H can be considered to be very close to 1, with possible deviations being at most 10%. However, in SnTe, it was shown that the contribution of the second, heavy valence band can result in deviations of r_H from 1 by up to 40% [S4,S5]. In addition, the RL may lead to additional variations in r_H due to the significant distortion of the valence band structure. In any case, even if the hole concentrations reported herein can show some deviations from the actual hole concentrations, this effect cannot account for the deviations of the present data from the Ioffe-Pisarenko curve and for the observed strong decrease in the mobility by an order of magnitude. Because at present exact calculations of r_H

are not possible, we thus made the reasonable assumption that $r_H = 1$ due to the degenerate nature of our samples.

Electronic structure calculations were done using the Korringa-Kohn-Rostoker (KKR) method with the coherent potential approximation (CPA), applied to account for the chemical disorder. The Munich SPR-KKR package was used [S6,S7]. The experimental rock-salt crystal structure and lattice parameter (a = 6.32 Å) were used. Regular k-point mesh was used in calculations, with 3000 k-points for the self-consistent cycle, $4 – 20\times10^5$ for the density of states (DOS) and Bloch spectral density functions (BSF) and $2 – 10\times10^6$ for conductivity calculations (number of points given in the irreducible part of the Brillouin zone, larger number of points were required for lower impurity concentrations). Conductivity calculations included the vertex corrections. The crystal potential was constructed in the framework of the local density approximation (LDA), using Vosko, Wilk and Nussair [S8] formula for the exchange-correlation part. For all atoms, angular momentum cut-off $l_{\max}$ = 3 was set and full-potential full-relativistic calculations were performed for DOS and BSF. For the conductivity calculations, spherical potential approximation was employed. High convergence limits were put on the self-consistent cycle (10^{-5} Ry for the Fermi level E_F and for the total energy). The position of E_F was obtained using the Lloyd formula.

3). Additional information about the Bloch spectral density functions (BSF)

Bloch spectral density functions $A(\boldsymbol{k}, E)$ allow to investigate the electronic dispersion relations in disordered materials, where electrons are scattered due to the lack of translational symmetry and presence of impurities (wave vector is not a conserved quantum number anymore). In such a case, the traditional description of the electronic structure, using the electronic dispersion relations $E(\boldsymbol{k})$, have to be generalized, and the KKR-CPA technique allows to do it by calculating BSF [S6,S9]. The meaning of BSF is sketched in **Figure S2.**

In the case of a perfect crystalline material (upper panel of Figure S2), BSF for a single wave vector $\mathbf{k_0}$ (and one spin direction) is a Dirac delta function of energy: $A(\boldsymbol{k_0}, E) = \delta(E - E_{\boldsymbol{k_0}})$, thus it is zero for all energies except the point E_0, where electron has its energy eigenvalue. The "peak" in the $\delta(E - E_{\boldsymbol{k_0}})$ function shows the position of an infinitely narrow electronic band, with infinite life time of the Bloch electrons (no scattering takes place at T = 0 K in a perfect crystal). The name "spectral density function" also describes another characteristic of the BSF as k-resolved density of states: the integral of $A(\boldsymbol{k_0}, E)$ over all energies is equal to 1, i.e. the number of electronic states available at $\boldsymbol{k_0}$ for each spin direction (in the case of a hypothetical

single-band material, while in the multi-band case, each band/BSF contributes 1 state per spin), and the integral over all $\boldsymbol{k}$ gives the usual density of states function [S9]. In non-magnetic materials, as in our case, BSFs are added for both spin directions, and the corresponding integrals are equal to 2.

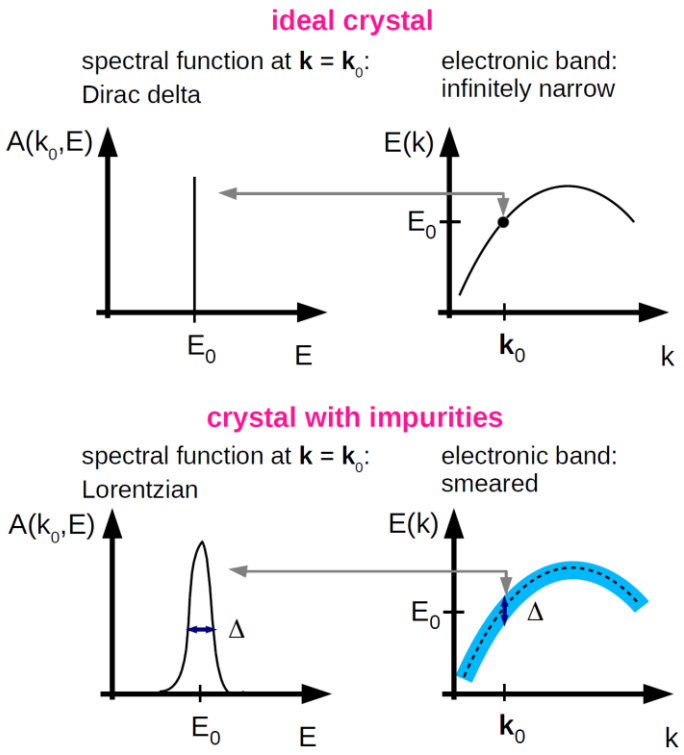

Figure S2. Schematic explanation of the relation between the Bloch spectral density functions $A(\boldsymbol{k}, E)$ and electronic bands E(**k**) in the case of idea crystal and crystal with impurities.

In the case where impurities are present in the material (bottom panel of **Figure S2**), spectral function broadens and in most cases it adopts the shape of the Lorentz function:

$$A(\boldsymbol{k_0}, E) = \frac{1}{\pi} \frac{\frac{1}{2}\Delta}{(E-E_0)^2 + \left(\frac{1}{2}\Delta\right)^2},$$

where E_0 is the Lorentzian peak position, which defines the band center, and Δ is the full width at half maximum (FWHM), which describes the strength of the impurity-induced scattering, visualized as the band smearing effect. In such a case, the electronic lifetime τ becomes finite and is related to the FWHM of the spectral function as $\tau = \frac{\hbar}{\Delta}$ [S10]. Of note, the electronic lifetime corresponds here to the Boltzmann relaxation time, the equivalence of which can be demonstrated within the KKR-CPA framework [S10]. The stronger is the impurity-induced scattering, the broader becomes the spectral function and more smeared the band structure

picture. The situation is more complicated for resonant impurities, as BSF becomes very broad and non-Lorentzian in shape (cf. **Figure 3**). As a consequence, relaxation time is not well defined, and thus, only rough estimations of τ may be obtained. This is the case studied in our work, as shown in **Figure 3**. Nevertheless, the Kubo-Greenwood formalism incorporated into KKR-CPA method [S6,S10] allows to calculate the T = 0 K electrical conductivity even for such a case.

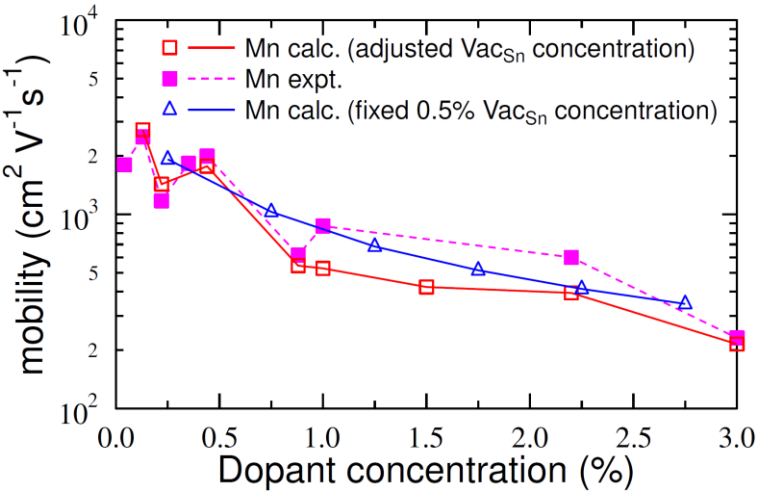

Figure S3. Charge carrier mobility as a function of the Mn content in $Sn_{1-x}Mn_xTe$, calculated in two ways: at each point, the Vac_{Sn} concentration was adjusted to match the carrier concentration to the experimental one (up to 1 %, see Table 1), or with 0.5% Vac_{Sn} concentration kept constant along the series. Comparison to the experimental points should be done using the "adjusted Vac_{Sn} concentration" series, while the calculation for the "fixed Vac_{Sn} concentration" series shows a smooth monotonic reduction of the hole mobility with increasing the Mn content. The experimental data points were taken from Refs. [S11,S12,S13]. The comparison between these datasets also shows that the uncertainty in vacancy concentrations does not significantly affect the observed trend.

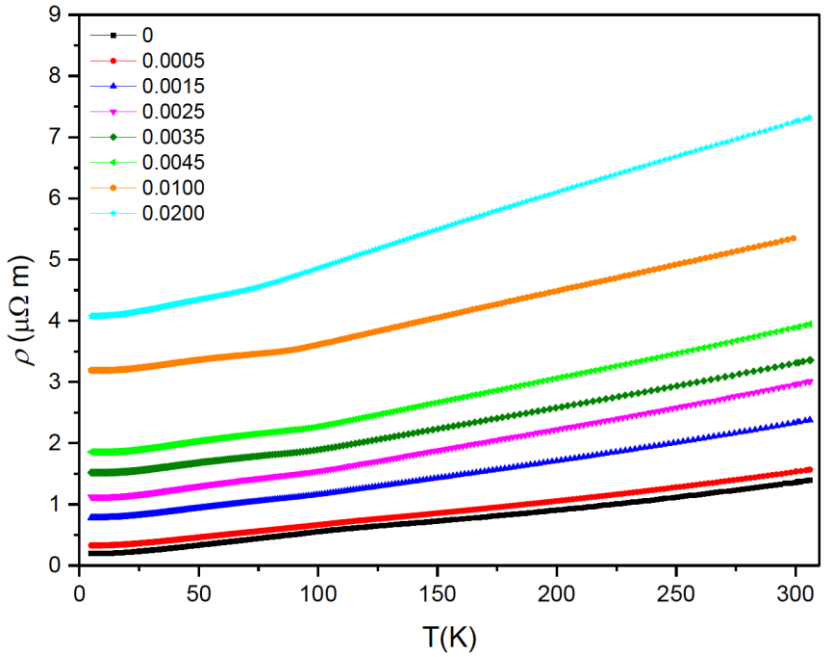

Figure S4. Temperature dependence of the electrical resistivity ρ of the polycrystalline samples $Sn_{1.03-x}In_xTe$ for $0.0 \leq x \leq 0.02$. The samples on which these data were measured are the same as those reported in our prior study [S3]. The change of slope, visible between 75 and 100 K for $x \geq 0.0025$, is likely due to the well-documented displacive ferroelectric transition [S14,S15,S16] that varies with the hole concentration. This transition is expected to only slightly affect the residual resistivity values. The metallic character that persists across the entire In concentration range evidences the absence of activated-like behavior at low temperatures that may arise from the presence of energy barriers at the grain boundaries [S17,S18], making the residual resistivity a well-defined and relevant quantity in the present series.

References

[S1] R. S. Allgaier, B. Houston, *Phys. Rev. B* 1972, **5**, 2186.

[S2] P. B. Littlewood, B. Mihaila, R. K. Schulze, D. J. Safarik, J. E. Gubernatis, A. Bostwick, E. Rotenberg, C. P. Opeil, T. Durakiewicz, J. L. Smith, J. C. Lashley, *Phys. Rev. Lett.* 2010, **105**, 086404.

[S3] S. Misra, B. Wiendlocha, J. Tobola, F. Fesquet, A. Dauscher, B. Lenoir, C. Candolfi, *J. Mater. Chem. C* 2020, **8**, 977.

[S4] R. F. Brebrick and A. J. Strauss, Phys. Rev. **1963**, 131, 104.

[S5] R. F. Brebrick, J. Phys. Chem. Solids **1963**, 24, 27.

[S6] H. Ebert, D. Ködderitzsch, J. Minár, *Rep. Prog. Phys.* 2011, **74**, 096501.

[S7] H. Ebert *et al.*, The Munich SPR-KKR package, version 7.7.3, **2019**. https://www.ebert.cup.uni-muenchen.de/index.php/en/software-en/13-sprkkr (accessed on 04.03.2021)

[S8] S. H. Vosko, L. Wilk and M. Nusair, *Can. J. Phys.*, 1980, **58**, 1200.

[S9] J. S. Faulkner and G. M. Stocks, *Phys. Rev. B* 1980, **21**, 3222.

[S10] W. H. Butler, *Phys. Rev. B* 1985**, 31**, 3260.

[S11] M. Inoue, H. Yagi, K. lshii, T. Tatsukawa *J. Low Temp. Phys.* 1976**, 23**, 785.

[S12] H. Chi, G. Tan, M.G. Kanatzidis, Q. Li, C. Uher, *Appl. Phys. Lett.* 2016, **108**, 182101.

[S13] M. Inoue, K. lshii, H. Yagi, T. Tatsukawa, *Memoirs of the Faculty of Engineering, Fukui University*, 1976, **24**, 237.

[S14] P. Littlewood, *J. Phys. C* 1980, **13**, 4855.

[S15] E. K. H. Salje, D. J. Safarik, K. A. Modic, J. E. Gubernatis, J. C. Cooley, R. D. Taylor, B. Mihaila, A. Saxena, T. Lookman, J. L. Smith, R. A. Fisher, M. Pasternak, C. P. Opeil, T. Siegrist, P. B. Littlewood, J. C. Lashley, *Phys. Rev. B* 2010, **82**, 184112.

[S16] C. D. O'Neill, D. A. Sokolov, A. Hermann, A. Bosak, C. Stock, A. D. Huxley, *Phys. Rev. B* 2017, **95**, 144101.

[S17] T. J. Slade, J. A. Grovogui, J. J. Kuo, S. Anand, T. P. Bailey, M. Wood, C. Uher, G. J. Snyder, V. P. Dravid, M. G. Kanatzidis, *Energy Environ. Sci.* 2020, **13**, 1509.

[S18] K. Imasato, C. Fu, Y. Pan, M. Wood, J. J. Kuo, C. Felser, G. J. Snyder, *Adv. Mater.* 2020, **32**, 1908218.